

Bayesian Focusing for Coherent Wideband Beamforming

Yaakov Bucris, *Student Member, IEEE*, Israel Cohen, *Senior Member, IEEE*, and Miriam A. Doron, *Member, IEEE*

Abstract—In this paper, we present and study a Bayesian focusing transformation (BFT) for coherent wideband array processing, which takes into account the uncertainty of the direction of arrivals (DOAs). The Bayesian focusing method minimizes the mean-square error of the transformation over the probability density functions (pdfs) of the DOAs, thus achieving improved focusing accuracy over the entire bandwidth. In order to solve the Bayesian focusing problem, we derive and utilize a weighted extension of the wavefield interpolated narrowband generated subspace (WINGS) focusing transformation. We provide a closed-form expression for the optimal BFT and extend it to the case of directional sensors. We then consider a numerical computation scheme of the BFT in the angular domain. We show that if an angular sampling condition is satisfied then the angle domain approximation yields the optimal BFT. We also treat the important issue of robust focused minimum variance distortionless response (MVDR) beamformer. We analyze the sensitivity of the focused MVDR to the focusing errors and show that the array gain (AG) is inversely proportional to the square of the signal-to-noise ratio (SNR) for large values of the SNR, and highly sensitive to the focusing errors. In order to reduce this sensitivity we generalize the popular narrowband diagonal loaded MVDR to the focused wideband case, referred to as the Q-loaded focused MVDR wideband beamformer. We derive a closed-form analytic expression for the AG of the Q-loaded focused MVDR beamformer which depends on the focusing transformations. A numerical performance evaluation and simulations demonstrate the advantage of the BFT over that of other focusing transformations, for multiple source scenarios.

Index Terms—Adaptive, Bayesian, beamforming, focusing, generalized loading, minimum variance distortionless response (MVDR), wideband.

I. INTRODUCTION

ADAPTIVE beamforming techniques are used to enhance the signal-to-interference plus noise ratio in many applications such as wireless communications, radar, sonar, acoustics, and seismic sensing. These techniques are effective in rejecting interference signals whose incident directions of arrivals (DOAs) on a sensor array differ from that of the desired

signals [1]. The potential of adaptive beamforming was already recognized since the early 1960s for the narrowband case. Yet, in the last two decades, the necessity for wideband adaptive beamforming increased with the development of third and fourth generations of wireless communications for mobile systems as well as ultra-wideband communication systems [2]–[5]. These systems support very high data rate communications due to their wideband nature combined with their space-time processing abilities.

Wideband adaptive beamforming techniques can be classified into two main categories. The first category consists of non-coherent beamforming methods implemented either in the time domain or in the frequency domain. The non-coherent time domain techniques utilize multi-tap spatial adaptive filters whose coefficients are adjusted to suppress the interferences while preserving the desired signal (e.g., [2], [6]–[8]). The non-coherent frequency domain techniques implement a narrowband adaptive beamformer in each frequency bin. These methods are computationally expensive, have a slow convergence rate due to a large number of adaptive coefficients, and are prone to signal cancellation problems in coherent source scenarios. The second category consists of coherent methods for wideband adaptive beamforming which incorporate a focusing procedure for signal subspace alignment [9]. The focusing procedure involves a pre-processor implemented as a linear transformation which focuses the signal subspaces at different frequencies to a single frequency, followed by a narrowband beamformer. The main benefits of the coherent methods are low computational complexity, the ability to combat the signal cancellation problem [10], [11] and improved convergence properties (see example in [12]).

Focusing for wideband array processing was originally proposed and studied for the application of direction finding (DF) [13] and e.g., [14]–[18]. For example, [16] and [18] carried out a performance analysis of the DOA estimation errors after focusing, [17] concentrated on robust auto-focusing for DOA estimation, and in [14] it was shown that signal subspace transformation (SST) matrices such as the rotational signal subspace (RSS) transformations provide a sufficient statistic for maximum-likelihood (ML) estimation of the DOAs. However, focusing for the purpose of adaptive beamforming is a different problem with different considerations. An insightful example demonstrating the difference between the two applications is given in Section VI, where we show that the array gain (AG) of the focused adaptive beamformer is inversely proportional to the variance of the focusing errors. Therefore, the SST and RSS transformations, which were proved to be optimal for DF applications in [14] since they provide a sufficient statistic for ML DOA estimation, are unsuitable for adaptive beamforming,

Manuscript received January 18, 2011; revised July 25, 2011; accepted October 19, 2011. Date of publication November 08, 2011; date of current version February 24, 2012. This work was supported by the Israel Science Foundation under Grant 1130/11. The associate editor coordinating the review of this manuscript and approving it for publication was Dr. Michael Lewis Seltzer.

Y. Bucris and I. Cohen are with the Department of Electrical Engineering, Technion—Israel Institute of Technology, Haifa 32000, Israel (e-mail: sbucris@gmail.com; icohen@ee.technion.ac.il).

M. A. Doron is with Rafael Advanced Defense Systems L.T.D, P.O.B 2250(270), Haifa 30121, Israel (e-mail: miridoron1@gmail.com).

Color versions of one or more of the figures in this paper are available online at <http://ieeexplore.ieee.org>.

Digital Object Identifier 10.1109/TASL.2011.2175384

since their focusing error is high. Therefore, in this work we concentrate on focusing matrices which are specifically designed to minimize the direct focusing error by employing *a priori* statistical information, thus expected to yield improved performance in the adaptive beamforming application.

There are two basic approaches to design focusing matrices. The first approach, referred to as the directional focusing approach, consists of methods which require *a priori* knowledge of the DOAs using them as focusing directions [9], [13], [19], [20]. The second approach consists of spatial interpolation methods which focus all angular directions [12], [21], [22] and will be referred to as the panoramic focusing approach. This approach is based on the observation that in a wavefield composed of plane waves, the spatial, and spectral parameters are related, since plane waves depend on the frequency only through the product kr . Therefore, a transformation of the array manifold between frequencies is equivalent to a spatial interpolation of the array, where the new spatial coordinates are scaled by the desired frequency ratio. The directional focusing methods theoretically achieve relatively low focusing errors but in practice are highly sensitive to DOA uncertainties. The panoramic focusing methods do not require any knowledge of DOAs; however, they typically exhibit higher error levels, since they attempt to focus all directions simultaneously. Furthermore, the spatial interpolation process, employed in the panoramic focusing, requires that the array satisfy a spatial sampling condition. For example, linear equispaces arrays should have a sensor spacing less than or equal to half a wavelength at the highest frequency of the processing band. The general sampling conditions for an array of arbitrary geometry are derived and discussed in [23], which also treats in detail the interesting circular array as a test case.

Most of the focusing methods in the academic literature belong to either the directional approach requiring *a priori* knowledge of the DOAs or the panoramic approach where no *a priori* knowledge is required. There are a few focusing methods which attempt to compromise between the directional approach and the panoramic approach. A numerical method for focusing within angular sectors is proposed and studied in [18], and a unitary focusing matrix which incorporates a deterministic weighting function is derived and studied in [17].

In this paper, we propose an optimal Bayesian approach for focusing transformation design, which takes into account the uncertainty of the DOAs by modeling them as random variables with a given prior statistics. The Bayesian focusing transformation (BFT) minimizes the mean-square error (MSE) of the transformation, thus achieving higher focusing accuracy over the entire bandwidth. The proposed Bayesian focusing transformation is a compromise between the directional focusing approach, which requires preliminary DOAs estimates, and the spatial interpolation-based panoramic focusing approach, which does not require any DOAs estimates. In fact, BFT is a generalization which includes the two approaches as special cases.

We derive a closed-form expression for the optimal BFT, which is based on an extension of the Wavefield Interpolated Narrowband Generated Subspace (WINGS) method [12]. However, the optimal BFT solution is conceptually and computationally more complex than the simple numerical angle

domain least squares (LS) solution. We derive an angular sampling condition and prove that if it is satisfied, then the numerical angle domain solution is identical to the optimal BFT, thus justifying the use of a simple practical numerical solution. We may note that in [24], a unitary Bayesian focusing scheme for single source focusing was proposed. A discrete approximate version of the probability function is employed leading to an approximated discrete solution. The solution presented in this work is a closed form accurate solution suitable to the case of multiple sources. In addition, unitary focusing transformations are less suitable to beamforming applications since they significantly increase the focusing error, as explained earlier in this section regarding the SST and RSS focusing transformations which are also unitary.

After the focusing procedure, one may apply any narrowband adaptive beamforming algorithm such as the well-known minimum variance distortionless response (MVDR) beamformer [25], which has a better resolution and interference rejection capabilities than the conventional beamformer, provided that the array manifold is perfectly known. However, in practice, there are some inaccuracies due to array calibration errors, DOAs errors [26], and covariance matrix estimation errors [27]. In the focused MVDR beamformer, the focusing error also comes into play and may deteriorate the performance considerably. We show analytically in Section VI that for high SNR values the AG is inversely proportional to σ_g^4 where σ_g is the focusing error and consequently highly sensitive to focusing errors. In order to reduce these sensitivities of the MVDR beamformer, we derive and employ an extension of the well-known diagonal loading method for the coherent wideband case. We refer to this solution as the Q-loading scheme in which we add a scaled matrix \mathbf{Q} to the covariance matrix before inversion, where the \mathbf{Q} matrix depends on the focusing transformation. A comparative performance analysis of several focusing schemes combined with the robust Q-loaded MVDR demonstrates the efficacy of the BFT.

The paper is organized as follows. In Section II, we formulate the problem of interest. In Section III, we present the Bayesian focusing approach. Section IV reviews the WINGS method and a weighted extension is derived and used to solve the Bayesian focusing problem. In Section V, we examine a numerical computation of the BFT in the angular domain and prove that it is equal, under certain sampling conditions, to the analytic closed form solution of the BFT. In Section VI, we analyze the sensitivity of the focused MVDR beamformer to focusing transformation errors, and derive a robust focused MVDR beamformer using a generalized-loading scheme. In Section VII, we present some simulation examples of the BFT focused MVDR beamformer and compare its performance to other focusing methods. In Section VIII, we show numerical examples of the sensitivity of the focused MVDR to focusing transformation errors in high SNR values. Section IX concludes our work.

II. PROBLEM FORMULATION

Consider an arbitrary array of N sensors sampling a wavefield generated by P statistically independent wideband sources, in the presence of additive noise. For simplicity, we

confine our discussion to the free and far field model. The signal at the output of the n th sensor can be written as

$$x_n(t) = \sum_{p=1}^P s_p(t - \tau_{np}) + n_n(t), \quad n = 1, \dots, N \quad (1)$$

where $\{s_p(t)\}_{p=1}^P$ and $\{n_n(t)\}_{n=1}^N$ denote the radiated wideband signals and the additive noise processes, respectively. The parameters $\{\tau_{np}\}$ are the delays associated with the signal propagation time from the p th source to the n th sensor. Let $\{\gamma_i\}_{i=1}^P$ be the DOAs of the sources, $\gamma \equiv \theta$ in 2-D and $\gamma \equiv (\theta, \varphi)$ in 3-D where θ is the azimuth angle and φ is the elevation angle. For simplicity, we restrict ourselves to the 2-D case. Each T seconds of received data are divided into K snapshots and transformed to the frequency domain yielding

$$\mathbf{x}_k(w_j) = \mathbf{A}_\theta(w_j)\mathbf{s}_k(w_j) + \mathbf{n}_k(w_j) \quad j = 1, 2, \dots, J, \quad k = 1, 2, \dots, K \quad (2)$$

where J is the total number of frequency bins used for the processing. The vectors $\mathbf{x}_k(w_j)$, $\mathbf{s}_k(w_j)$, and $\mathbf{n}_k(w_j)$ denote vectors whose elements are the discrete Fourier coefficients of the measurements, the unknown signals and the noise, respectively, at the k th snapshot and at frequency w_j . The $N \times P$ matrix $\mathbf{A}_\theta(w_j)$ is the direction matrix

$$\mathbf{A}_\theta(w_j) \equiv [\mathbf{a}_{\theta_1}(w_j), \mathbf{a}_{\theta_2}(w_j), \dots, \mathbf{a}_{\theta_P}(w_j)]. \quad (3)$$

The vector $\mathbf{a}_\theta(w)$, referred to as the *array manifold* vector, is the response of the array to an incident plane wave at frequency w and DOA θ . For an array comprised of identical omnidirectional uncoupled sensors in free field, the *array manifold* vector is

$$[\mathbf{a}_\theta(w)]_m = \exp\{ikr_m \cdot \hat{\theta}\} \quad (4)$$

where $\hat{\theta} = \cos\theta\hat{x} + \sin\theta\hat{y}$ denotes a unit vector pointed towards the direction θ , and $k = w/c$ is the wave number associated with the frequency w . The vector \mathbf{r}_m marks the coordinates of the m th sensor. We assume that the noise vectors $\mathbf{n}_k(w_j)$ and the signal vectors $\mathbf{s}_k(w_j)$ are independent samples of a stationary, zero mean circular complex Gaussian random process, with unknown covariance matrices $\sigma_n^2(w_j)\mathbf{I}$ and $\mathbf{R}_s(w_j)$, respectively. The noise process is assumed to be uncorrelated with the signal process and the wideband sources are assumed to share a common bandwidth. Due to the broadband nature of the sources, using coherent processing is advantageous as discussed in the previous section. Let $\mathbf{T}(w_j)$ denote a transformation that maps the wideband array output from frequency w_j to the focusing frequency w_0 , so that the signal direction matrices are aligned across the frequency bandwidth

$$\mathbf{T}(w_j)\mathbf{A}_\theta(w_j) \cong \mathbf{A}_\theta(w_0) \quad (5)$$

i.e., $\mathbf{T}(w_j)$ transforms the *array manifold* from frequencies $\{w_j\}$ to the focusing frequency w_0 . Following [10], we may construct the focused time-domain vector $\mathbf{y}_k(n)$ as

$$\begin{aligned} \mathbf{y}_k(n) &= \sum_{j=1}^J \mathbf{T}(w_j)\mathbf{x}_k(w_j)e^{iw_jnT_s} \\ &\cong \mathbf{A}_\theta(w_0)\mathbf{s}(n) + \tilde{\mathbf{n}}(n) \end{aligned} \quad (6)$$

where $\mathbf{s}(n)$ is the vector of wideband unknown time domain signals within the focused frequency band $[w_1 : w_J]$, T_s is the sampling frequency and $\tilde{\mathbf{n}}(n)$ is the transformed noise. We note that the temporal focused vector $\mathbf{y}_k(n)$ has a narrowband array manifold while preserving the wideband spectral content of the signals. This allows the use of any narrowband adaptive beamformer matched to frequency w_0 , such as the MVDR beamformer. In the following, we describe a framework example for the MVDR adaptive beamformer using the sample matrix inversion (SMI) implementation. Let us first review the non-coherent wideband MVDR beamformer and then, describe the focused wideband MVDR beamformer.

A. Non-Coherent Adaptive Beamformer

The non-coherent wideband MVDR—SMI method is implemented in the frequency domain by applying a narrowband beamformer at each frequency bin (see, e.g., [1]). A discrete Fourier transform (DFT) is first performed followed by the computation of the narrowband sample covariance matrix at each frequency bin

$$\hat{\mathbf{R}}_x(w_j) = \frac{1}{K} \sum_{k=1}^K \mathbf{x}_k(w_j)\mathbf{x}_k^H(w_j). \quad (7)$$

The narrowband MVDR—SMI adaptive weight vector is then computed at each frequency bin as

$$\hat{\mathbf{w}}_\theta(w_j) = \frac{\hat{\mathbf{R}}_x^{-1}(w_j)\mathbf{a}_\theta(w_j)}{\mathbf{a}_\theta^H(w_j)\hat{\mathbf{R}}_x^{-1}(w_j)\mathbf{a}_\theta(w_j)}. \quad (8)$$

The adaptive weights (8) may now be used to perform the actual beamforming at each frequency bin yielding the non-coherent adaptive beamformer output, in the frequency domain. Finally, we note that beamformer (8) is sometimes referred to as the minimum power distortionless response (MPDR) method (see, e.g., [1]).

B. Coherent Focused Adaptive Beamformer

The MVDR-SMI focused adaptive beamformer may be simply implemented as a narrowband adaptive beamformer operating on the temporal focused data vector $\mathbf{y}_k(n)$ (6) whose focused sample covariance matrix is constructed by

$$\hat{\mathbf{R}}_x^f = \frac{1}{KJ} \sum_{k,n} \mathbf{y}_k(n)\mathbf{y}_k^H(n). \quad (9)$$

The focused coherent adaptive beamformer MVDR weight vector is simply computed in the time domain by

$$\hat{\mathbf{w}}_{\theta}^f = \frac{\left(\hat{\mathbf{R}}_x^f\right)^{-1} \mathbf{a}_{\theta}(w_0)}{\mathbf{a}_{\theta}^H(w_0) \left(\hat{\mathbf{R}}_x^f\right)^{-1} \mathbf{a}_{\theta}(w_0)} \quad (10)$$

where w_0 is the focusing frequency and f stands for *focused* beamformer.

In this paper, we are interested in finding a focusing transformation $\mathbf{T}(w_j)$ which can handle DOA uncertainties while achieving the minimal mean-square focusing error at the true DOAs. To this end, we use a Bayesian approach employing a statistical model where the DOAs $\{\theta_i\}_{i=1}^P$ are modeled as statistically independent random variables. We then define and solve the Bayesian focusing problem for wideband arrays.

III. BAYESIAN FOCUSING TRANSFORMATION (BFT)

In this section, we consider the case of DOAs uncertainties. We use a Bayesian model in order to define the optimal minimum mean square error (MMSE) focusing transformation $\mathbf{T}_{BFT}(w_j)$ as the solution to the following minimization problem:

$$\mathbf{T}_{BFT}(w_j) = \arg \min_{\mathbf{T}(w_j)} E_{\boldsymbol{\theta}} \left\{ \|\mathbf{A}_{\boldsymbol{\theta}}(w_0) - \mathbf{T}(w_j) \mathbf{A}_{\boldsymbol{\theta}}(w_j)\|_F^2 \right\} \quad (11)$$

where w_0 is the focusing frequency, $\|\cdot\|_F$ denotes the Frobenious norm, and $E_{\boldsymbol{\theta}} \{\cdot\}$ denotes the expectation over the statistical distribution of the DOA vector $\boldsymbol{\theta}$. Assuming $\{\theta_i\}_{i=1}^P$ are statistically independent random variables, it can be proved that

$$\begin{aligned} & E_{\boldsymbol{\theta}} \left\{ \|\mathbf{A}_{\boldsymbol{\theta}}(w_0) - \mathbf{T}(w_j) \mathbf{A}_{\boldsymbol{\theta}}(w_j)\|_F^2 \right\} \\ &= \int_{\theta=-\pi}^{\pi} d\theta_1 \dots d\theta_P f_{\theta_1}(\theta_1) \dots f_{\theta_P}(\theta_P) \cdot \\ & \sum_{i=1}^P \|\mathbf{a}_{\theta_i}(w_0) - \mathbf{T}(w_j) \mathbf{a}_{\theta_i}(w_j)\|^2 \\ &= \int_{\theta=-\pi}^{\pi} d\theta \|\mathbf{a}_{\theta}(w_0) - \mathbf{T}(w_j) \mathbf{a}_{\theta}(w_j)\|^2 \sum_{i=1}^P f_{\theta_i}(\theta) \quad (12) \end{aligned}$$

where $\|\cdot\|$ is the Euclidian norm and $f_{\theta_i}(\theta)$ denote the probability density functions (pdfs) of the i th DOA. Defining

$$\rho^2(\theta) \triangleq \sum_{i=1}^P f_{\theta_i}(\theta) \quad (13)$$

and substituting (13) into the right-hand side of (12) yields the following integral to be minimized:

$$\begin{aligned} & \mathbf{T}_{BFT}(w_j) \\ &= \arg \min_{\mathbf{T}(w_j)} \int_{\theta=-\pi}^{\pi} d\theta \|\rho(\theta) (\mathbf{a}_{\theta}(w_0) - \mathbf{T}(w_j) \mathbf{a}_{\theta}(w_j))\|^2. \quad (14) \end{aligned}$$

Note that (14) is a generalized form which includes many focusing schemes as private cases. It reduces to the panoramic focusing scheme, e.g., WINGS [12] by taking a uniform distribution, i.e., $\rho(\theta) \equiv 1$. Taking $\rho(\theta) = \sum_i \delta(\theta - \hat{\theta}_i)$ yields the directional focusing matrices originally proposed by Hung and Kaveh [9], which focus at discrete angles taken to be the preliminary estimates of the DOAs $\{\hat{\theta}_i\}_{i=1}^P$. Note also that in (14) one may use either the *a priori* pdfs of the DOAs as $f_{\theta_i}(\theta)$, or the *a posteriori* pdfs, estimated from the received data. The first approach yields a data independent transformation, while the second approach requires estimation of the conditional pdfs from the data yielding a data dependent transformation. The reader can refer to [28] where a time progressing algorithm employing the *a posteriori* pdfs was proposed. In Section IV, we derive a closed form expression for the BFT solving (14), utilizing a weighted extension of the WINGS [12] focusing method.

IV. BFT AS A WEIGHTED EXTENSION OF THE WINGS

In this section, we first review the main points of the WINGS, then we develop a weighted extension of the WINGS, for the 2-D case, which incorporates an arbitrary angular weighting function $\rho(\theta)$. Finally, we use the closed form expression of the weighted WINGS extension to solve (14).

A. Wings

The WINGS focusing method [12] is based on the wavefield modeling formalism [23] according to which, the output of almost any array $\mathbf{x}(w)$ of arbitrary geometry can be written as a product of array geometry dependent part and wavefield dependent part, i.e., $\mathbf{x}(w) = \mathbf{G}(w) \boldsymbol{\psi}(w)$ where $\mathbf{G}(w) = [\dots, \mathbf{g}_{-1}(w), \mathbf{g}_0(w), \mathbf{g}_1(w), \dots]$ is the array sampling matrix which is independent of the wavefield and $\boldsymbol{\psi}(w)$ is the coefficient vector representing the wavefield. The vector $\boldsymbol{\psi}(w)$ contains the orthogonal decomposition coefficients of the wavefield function $\Psi(w, \mathbf{r})$ [23] where $\Psi(w, \mathbf{r})$ is a Fourier component of the temporal wavefield function $\Psi(t, \mathbf{r})$ and satisfies the source free *Helmholtz equation*:

$$(\nabla^2 + k^2) \Psi(w, \mathbf{r}) = 0. \quad (15)$$

Since we assumed a far field scenario, we can write the wavefield as a linear combination of plane waves

$$\Psi(w, \mathbf{r}) = \int_{\Theta} d\theta \eta(\theta) e^{j k \mathbf{r} \hat{\boldsymbol{\theta}}} \quad (16)$$

where $\eta(\theta) \in \mathbf{L}_2(\Theta)$ is the *radiation density* in the direction θ . We can define \hat{H} as the Hilbert space of allowed wavefields of the form (16) with $\eta(\theta) \in \mathbf{L}_2(\Theta)$ and it can be shown that there exist an isomorphism between \hat{H} and $\mathbf{L}_2(\Theta)$. Each column in the sampling matrix $\mathbf{G}(w)$ is the array response to a basis function belongs to an orthogonal basis set in \hat{H} and depends only in the array geometry. Using the wavefield modeling formalism,

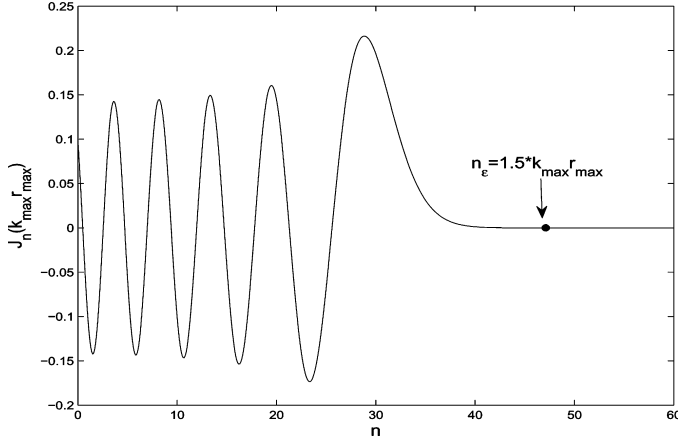


Fig. 1. Example of a Bessel function behavior as a function of its order. The asterisk indicates the order n_ε used in our simulations.

the steering vector can be expressed in terms of its orthogonal decomposition

$$\mathbf{a}_\theta(w) = \sum_n \mathbf{g}_n(w) h_n^*(\theta) \quad (17a)$$

$$\mathbf{g}_n(w) = \int_{\Theta} \mathbf{a}_\theta(w) h_n(\theta) d\theta \quad (17b)$$

where $\Theta = [-\pi, \pi]$ is the manifold of possible DOAs and $\{h_n(\theta)\}_{n=-\infty}^{\infty}$ is an orthogonal basis set in $\mathbf{L}_2(\Theta)$. In 2-D, we use the Fourier basis, i.e., $h_n(\theta) = (1/\sqrt{2\pi})e^{-in\theta}$, $\theta \in \Theta$. Inserting expression (4) into (17b) yields for the 2-D case and omnidirectional and uncoupled sensors

$$\begin{aligned} \mathbf{G}_{mn}(w) &= \int_{\Theta} e^{ikr_m \cdot \hat{\theta}} h_n(\theta) d\theta \\ &\stackrel{2-D}{=} \sqrt{2\pi} (i)^n J_n(kr_m) e^{-in\theta_m} \end{aligned} \quad (18)$$

where (θ_m, r_m) designate the polar coordinates of the m th sensor, and $J_n(kr)$ denotes the Bessel function of the first kind. We should point out that although $\mathbf{G}(w)$ has an infinite number of columns, we can see from (18) that there is an effective cutoff for $n \gg k_{\max} r_{\max}$, where $k_{\max} r_{\max}$ denotes the maximal value of kr for the given geometry and bandwidth, since for $n \gg kr$, the Bessel function $J_n(kr)$ decreases faster than exponentially to zero [29]. Let n_ε be defined by

$$|J_n(k_{\max} r_{\max})| < \varepsilon, \text{ for } n > n_\varepsilon \quad (19)$$

for some small ε of our choice. In Fig. 1, a graphic description of a Bessel function's behavior as a function of its order is presented for $k_{\max} r_{\max} = 31.4$ suitable to a linear array of $N = 20$ sensors and spectrum between $F_{\text{low}} = 1200$ Hz and $F_{\text{high}} = 1800$ Hz. One can see that for this example, a selected truncation order $n_\varepsilon = 1.5k_{\max} r_{\max} \approx 50$ yielding $\varepsilon = 2.4e-6$ is justified, and will be used in our simulations.

A quantitative evaluation of the error caused by the Bessel function's truncation is given in [23]. It proves that by this choice, the truncation error is negligible in comparison to other errors caused by the focusing operation, which are treated later in this work. From now on, we use the truncated version of the sampling matrix $\mathbf{G}(w)$ which is now an $N \times (2n_\varepsilon + 1)$ matrix.

The WINGS focusing transformation $\mathbf{T}(w_j)$ minimizes ε_j , the L_2 norm of the focusing error $\mathbf{e}_\theta(w_j)$ over all possible directions

$$\varepsilon_j^2 \triangleq \frac{1}{N} \int_{\theta=-\pi}^{\pi} d\theta \|\mathbf{e}_\theta(w_j)\|^2 \quad (20)$$

where

$$\mathbf{e}_\theta(w_j) = \mathbf{a}_\theta(w_0) - \mathbf{T}(w_j) \mathbf{a}_\theta(w_j) \quad \forall \theta. \quad (21)$$

Using (17a), the error can be expressed as

$$\mathbf{e}_\theta(w_j) = [\mathbf{G}(w_0) - \mathbf{T}(w_j) \mathbf{G}(w_j)] \mathbf{h}_\theta \quad (22)$$

where the vector \mathbf{h}_θ contains the basis functions $\{h_n(\theta)\}$ as its elements which comprise a complete and orthogonal basis set over $\mathbf{L}_2(\Theta)$. Thus, one may consider (22) to be the orthogonal decomposition of the error vector $\mathbf{e}_\theta(w_j)$. We can use Parseval's identity and derive the equivalent least-square (LS) minimization problem

$$\varepsilon_j^2 = \frac{1}{N} \|\mathbf{G}(w_0) - \mathbf{T}(w_j) \mathbf{G}(w_j)\|_F^2. \quad (23)$$

The WINGS focusing matrix minimizing (23) is given by

$$\mathbf{T}_{\text{WINGS}}(w_j) = \mathbf{G}(w_0) \mathbf{G}^\dagger(w_j) \quad (24)$$

where \mathbf{G}^\dagger denotes the pseudo-inverse of \mathbf{G} .

B. Weighted Wings

In this section, we extend the WINGS minimization problem (20) to incorporate an arbitrary angular weighting function $\rho(\theta)$, which will be used later on to solve the Bayesian focusing problem (14). Let $\tilde{\varepsilon}_j$ be the weighted L_2 norm of the focusing error $\mathbf{e}_\theta(w_j)$

$$\begin{aligned} \tilde{\varepsilon}_j^2 &= \frac{1}{N} \int_{\Theta} d\theta \|\rho(\theta) \mathbf{e}_\theta(w_j)\|^2 \\ &= \frac{1}{N} \int_{\Theta} d\theta \|\rho(\theta) (\mathbf{a}_\theta(w_0) - \mathbf{T}(w_j) \mathbf{a}_\theta(w_j))\|^2. \end{aligned} \quad (25)$$

In order to find the transformation minimizing (25) let us find $\mathbf{C}(w)$, the orthogonal decomposition of the product $\rho(\theta) \mathbf{a}_\theta(w)$

$$[\mathbf{C}(w)]_{mn} \equiv \int_{\theta=-\pi}^{\pi} d\theta \rho(\theta) [(\mathbf{a}_\theta(w))_m h_n(\theta)]. \quad (26)$$

Let $\rho(\theta) = \sum_n \rho_n h_n(\theta)$ be the orthogonal decomposition of the angular weighting function $\rho(\theta)$, then substituting (17a) into (26) we may write

$$\begin{aligned} [\mathbf{C}(w)]_{mn} &= \int_{\theta=-\pi}^{\pi} d\theta \sum_p \rho_p h_p(\theta) \sum_l \mathbf{G}_{ml}(w) h_l^*(\theta) h_n(\theta) \\ &= \sum_{p,l} \rho_p \mathbf{G}_{ml}(w) \int_{\theta=-\pi}^{\pi} d\theta h_n(\theta) h_p(\theta) h_l^*(\theta). \end{aligned} \quad (27)$$

In the 2-D case $h_n(\theta)$ are the Fourier functions and

$$\int_{\theta=-\pi}^{\pi} d\theta h_n(\theta) h_p(\theta) h_l^*(\theta) = \frac{1}{\sqrt{2\pi}} \delta_{n+p-l} \quad (28)$$

which yields the following convolution expression:

$$[\mathbf{C}(w)]_{mn} = \frac{1}{\sqrt{2\pi}} \sum_p \rho_p \mathbf{G}_{m,n+p}(w). \quad (29)$$

We now insert into (25) the orthogonal decomposition $\rho(\theta) \mathbf{a}_\theta(w) = \mathbf{C}(w) \mathbf{h}_\theta$ and get the following minimization integral

$$\tilde{\varepsilon}_j^2 = \frac{1}{N} \int_{\theta=-\pi}^{\pi} d\theta \|\mathbf{C}(w_0) - \mathbf{T}(w_j) \mathbf{C}(w_j)\| \mathbf{h}_\theta\|^2. \quad (30)$$

Using Parseval's identity we get

$$\tilde{\varepsilon}_j^2 = \frac{1}{N} \|\mathbf{C}(w_0) - \mathbf{T}(w_j) \mathbf{C}(w_j)\|_F^2. \quad (31)$$

Thus, the weighted WINGS transformation minimizing $\tilde{\varepsilon}_j$ is given by the LS solution minimizing (31)

$$\mathbf{T}(w_j) = \mathbf{C}(w_0) \mathbf{C}^\dagger(w_j). \quad (32)$$

Since (25) has exactly the same form as (14), we get the closed form expression for the MMSE optimal BFT

$$\mathbf{T}_{BFT}(w_j) = \mathbf{C}(w_0, \rho(\theta)) \mathbf{C}^\dagger(w_j, \rho(\theta)) \quad (33)$$

where $\rho(\theta)$ is given by (13).

C. Directional Sensors and Empirically Calibrated Arrays

In this section, we provide a useful extension of BFT and WINGS focusing for the case of directional sensors and empirically calibrated arrays. Let $d^m(\theta)$ denote the directivity pattern of the m th, which may be known *a priori* or empirically measured, and let us define the directional array manifold $[\tilde{\mathbf{a}}_\theta(w)]_m = d^m(\theta) [\mathbf{a}_\theta(w)]_m$. One can verify that the matrix $\mathbf{C}(w)$ in the BFT solution (33) is now given by $\tilde{\mathbf{C}}(w)$, the orthogonal decomposition of weighted directional array manifold $\rho(\theta) \tilde{\mathbf{a}}_\theta(w)$

$$[\tilde{\mathbf{C}}(w)]_{mn} = \frac{1}{\sqrt{2\pi}} \sum_p \tilde{\rho}_p^m \mathbf{G}_{m,n+p}(w). \quad (34)$$

where $\{\tilde{\rho}_p^m\}$ are the Fourier coefficients of the composite weighting function $\tilde{\rho}^m(\theta) = \rho(\theta) d^m(\theta)$ incorporating the sensor directivity function.

The optimal BFT solution (33) based on the weighted WINGS and the wavefield formalism is computationally complex. In Section V, we examine an efficient numerical computation of the BFT performed in the angular domain. We also prove that under certain sampling conditions the numerical computation yields the accurate BFT transformation.

V. BFT COMPUTATION IN THE ANGULAR DOMAIN

In this section, we address the numerical approximate computation of the BFT in the angular domain. The numerical solution can be derived simply by a discrete sum approximation of the integral in (14), obtained by sampling the angular variable θ

$$\begin{aligned} \hat{\mathbf{T}}_{BFT}^L(w_j) \\ = \arg \min_{\mathbf{T}(w_j)} \sum_{l=0}^{L-1} \|\rho(\theta_l) (\mathbf{a}_{\theta_l}(w_0) - \mathbf{T}(w_j) \mathbf{a}_{\theta_l}(w_j))\|^2. \end{aligned} \quad (35)$$

The BFT approximation is computed as the LS solution of (35) in the angle domain. We will show that if an angular sampling condition is satisfied then the angle domain approximation (35) is equal to the optimal BFT computed by the weighted WINGS transformation (33).

The following claim links the sampling matrix $\mathbf{G}(w)$ defined by (17b) to the sampled array manifold matrix via the DFT relationship.

1) *Claim 1:* Let $\mathbf{A}_L(w)$ be the $N \times L$ matrix constructed by sampling the array manifold $\mathbf{a}_\theta(w)$ at $\theta_l = (2\pi/L)l$, $l = 0, 1, \dots, L-1$. If $L \geq l_g$, where l_g is the row length of $\mathbf{G}(w)$, then, for the 2-D case, $\mathbf{A}_L(w)$ and $\mathbf{G}(w)$ are related by the $l_g \times L$ DFT matrix \mathbf{F}_L

$$\mathbf{A}_L(w) = \mathbf{G}(w) \mathbf{F}_L \quad (36a)$$

$$\mathbf{G}(w) = \mathbf{A}_L(w) \mathbf{F}_L^H \quad (36b)$$

where $[\mathbf{F}_L]_{mn} = (1/\sqrt{2\pi}) e^{i2\pi mn/L}$.

Proof: For $L \geq l_g$ the DFT analysis (36a) is simply the matrix formulation of (17a) for the 2-D case. The proof for (36b) results from applying the well-known condition for frequency domain sampling and reconstruction of finite length discrete time signals, see, e.g., [30]. The DFT synthesis (36b) is valid only if $L \geq l_g$. \square

Note that l_g is equal to $(2n_\varepsilon + 1)$, where n_ε is the effective cutoff index of \mathbf{G} defined using the wavefield formalism by (19). For example if we choose $n_\varepsilon = 1.5k_{\max} r_{\max}$ we get the condition $L \geq 3k_{\max} r_{\max} + 1$.

In a similar manner we can write a second claim linking the weighted array manifold vector $\rho(\theta_l) \mathbf{a}_{\theta_l}(w)$ to its orthogonal decomposition matrix $\mathbf{C}(w)$ defined by (26) via the DFT relationship.

2) *Claim 2:* Let $\tilde{\mathbf{A}}_L^p(w)$ be the $N \times L$ matrix whose l th column is the weighted array manifold vector $\rho(\theta_l) \mathbf{a}_{\theta_l}(w)$ where $\theta_l = (2\pi/L)l$, $l = 0, 1, \dots, L-1$. If $L \geq l_c$, where l_c

is the row length of $\mathbf{C}(w)$, then, for the 2-D case, $\tilde{\mathbf{A}}_L^\rho(w)$ and $\mathbf{C}(w)$ are related by the $l_c \times L$ DFT matrix \mathbf{F}_L

$$\tilde{\mathbf{A}}_L^\rho(w) = \mathbf{C}(w)\mathbf{F}_L \quad (37a)$$

$$\mathbf{C}(w) = \tilde{\mathbf{A}}_L^\rho(w)\mathbf{F}_L^H. \quad (37b)$$

The row-length of $\mathbf{C}(w)$ can be evaluated from the convolution (29) as the sum $2n_\varepsilon + n_\rho$, where n_ρ is the number of the Fourier coefficients $\{\rho_n\}$ of the angular weighting function $\rho(\theta)$.

One can easily verify that $\hat{\mathbf{T}}_{BFT}^L(w_j)$ solving (35) is given by

$$\hat{\mathbf{T}}_{BFT}^L(w_j) = \tilde{\mathbf{A}}_L^\rho(w_0) \left(\tilde{\mathbf{A}}_L^\rho(w) \right)^\dagger. \quad (38)$$

The following theorem links the numerical angle domain approximate transformation defined above to the optimal BFT computed by the weighted WINGS solution (33).

Theorem: The LS angle domain BFT approximation $\hat{\mathbf{T}}_{BFT}^L(w_j)$ minimizing (35) is equal to the optimal BFT, $\mathbf{T}_{BFT}(w_j)$ minimizing (25) if

$$L \geq 2n_\varepsilon + n_\rho. \quad (39)$$

Proof: If $L \geq 2n_\varepsilon + n_\rho$ we can use claim 2 and substitute (37b) into (33) and using (38) we get

$$\begin{aligned} \mathbf{T}_{BFT}(w_j) &= \mathbf{C}(w_0, \rho(\theta))\mathbf{C}^\dagger(w_j, \rho(\theta)) \\ &= \tilde{\mathbf{A}}_L^\rho(w_0)\mathbf{F}_L^H \left(\tilde{\mathbf{A}}_L^\rho(w_j)\mathbf{F}_L^H \right)^\dagger \\ &= \tilde{\mathbf{A}}_L^\rho(w_0) \left(\tilde{\mathbf{A}}_L^\rho(w_j) \right)^\dagger \\ &= \hat{\mathbf{T}}_{BFT}^L(w_j). \end{aligned} \quad (40)$$

□

This theoretic result is useful since it justifies a simple straightforward angle-domain LS computation of the BFT using (38) without loss of accuracy. Note that the angular sampling condition on L is based on the wavefield formalism and the sampling matrix representation of a given array.

For the case of directional sensors, one can verify that condition (39) is still valid with n_ρ replaced by $\bar{n}_\rho = \max_m \{ \text{length}(\{\tilde{\rho}_p^m\}) \}$ the maximal length of the Fourier coefficients of the composite weighting function $\tilde{\rho}^m(\theta)$.

In Sections VI–IX, we proceed to conducting an analytic and simulative performance analysis of the focused MVDR beamformer as a function of the various focusing transformations. We first analyze the sensitivity of the focused MVDR to focusing errors and present a robust loaded form for the focused MVDR beamformer.

VI. Q-LOADED MVDR FOCUSED BEAMFORMER

In this section, we treat the issue of robust wideband focused MVDR beamforming. In the focused MVDR, the focusing errors often cause a significant deterioration at high SNR values (see simulation examples in the numerical Section VII). In the following, we attempt to provide some insight to the performance degradation in high SNR due to focusing errors, by an-

alytically studying the single-source case for single frequency focusing.

A. Sensitivity of the Focused MVDR Beamformer to Focusing Errors

In this section, we examine the effect of the focusing errors introduced by focusing from frequency w_j to frequency w_0 for a single source with single frequency focusing. We statistically model the focusing error and show analytically how the AG decreases as the SNR increases in the presence of focusing errors. The following analysis is based on modeling the focusing errors as small random independent complex perturbations of the array gains of the focused steering vector. A similar model has been used in [31], in order to analyze the sensitivity of the MVDR to amplitude and phase errors of the sensors. Let us write the m th element of the focused array manifold vector from frequency w_j to w_0 as

$$\begin{aligned} [\mathbf{T}(w_j)\mathbf{a}_\theta(w_0)]_m &= a_{\theta,m}^f(w_0, w_j) \\ &= [\mathbf{a}_\theta(w_0)]_m (1 + \Delta g_m(w_j)) \end{aligned} \quad (41)$$

where $[\mathbf{a}_\theta(w_0)]_m$ is defined by (4), and $\Delta g_m(w_j)$ represents a zero-mean circular complex Gaussian gain error of the m th sensor. We assume that the random gain errors are independent from sensor to sensor and have the same variance $\sigma_g^2(w_j)$

$$\sigma_g^2(w_j) \triangleq E \left[|\Delta g_m(w_j)|^2 \right], \quad m = 1, \dots, N \quad (42)$$

The focused data vector at frequency w_j is given by

$$\mathbf{x}^f(w_j) = s(w_j)\mathbf{a}_\theta^f(w_0, w_j) + \mathbf{T}(w_j)\mathbf{n}(w_j) \quad (43)$$

where $s(w_j)$ is the desired signal component at frequency w_j , and $\mathbf{n}(w_j)$ is the additive noise at frequency w_j . For the sake of simplicity we assume $\mathbf{T}(w_j)$ to be unitary, then under the model assumptions in Section II the focused covariance matrix $\mathbf{R}_x^f(w_j, w_0)$ is given by

$$\mathbf{R}_x^f(w_j, w_0) = \sigma_s^2(w_j)\mathbf{a}_\theta^f(w_0, w_j)(\mathbf{a}_\theta^f(w_0, w_j))^H + \sigma_n^2(w_j)\mathbf{I} \quad (44)$$

where $\sigma_s^2(w_j)$ is the power of the desired signal at w_j . The weight vector of the focused MVDR beamformer is given by

$$\mathbf{w}_\theta^f = \frac{(\mathbf{R}_x^f(w_j, w_0))^{-1}\mathbf{a}_\theta(w_0)}{\mathbf{a}_\theta^H(w_0)(\mathbf{R}_x^f(w_j, w_0))^{-1}\mathbf{a}_\theta(w_0)}. \quad (45)$$

Following [31] it can be shown that the output AG of the focused MVDR beamformer is given by

$$\begin{aligned} \text{AG} &= \frac{N + \sigma_g^2}{(1 + (N - 1)\sigma_g^2\xi)^2 + (N - 1)(N + \sigma_g^2)\sigma_g^2\xi^2} \\ &\xrightarrow{\xi, N \gg 1, N \gg \sigma_g^2 > 0} \frac{1}{\xi^2 N \sigma_g^2 (1 + \sigma_g^2)} \end{aligned} \quad (46)$$

where ξ is the input SNR. In Section VIII, we will examine the quality of (46) by comparing it to the analytic AG which will be derived in the Appendix. Equation (46) indicates that the output AG is inversely proportional to ξ^2 for $\xi \gg 1$ and inversely proportional to $\sigma_g^2(1 + \sigma_g^2)$ for $N \gg 1$ and $N \gg \sigma_g^2 > 0$, i.e., the AG is highly sensitive to the focusing errors. These results

stress the importance of using a robust MVDR scheme for the focused beamformer in addition to minimizing the focusing errors at the desired DOAs. We now proceed to present an extension of the narrowband robust MVDR beamformer to the focused wideband case using a generalized loading scheme, which brings into account the focusing transformations.

B. Robust MVDR Focused Beamformer by Q-Loading

In practice, due to array calibration errors and inaccurate knowledge of the source direction, it is often the case that the performance of the MVDR beamformer may deteriorate below that of the conventional beamformer [26]. Furthermore, the MVDR-SMI implementation is sensitive to estimation errors in the sample covariance matrix [27]. One of the popular methods to improve the robustness of the MVDR beamformer is the diagonal loading scheme [1], [27], [32], [33]. It is derived by imposing an additional quadratic constraint either on the Euclidian norm of the weight vector itself or on its difference from the nominal weight vector which is equivalent to limiting the white noise array gain. In this section we extend the popular well known diagonal loading scheme to the focused wideband MVDR. We note that many effective loading schemes exist in the literature, e.g., [19], [34], which may also be extended to the wideband case in a similar manner.

In the case of the focused beamformer, the output noise power is given by

$$\sigma_{n_{out}}^2 = \sigma_n^2 (\mathbf{w}_\theta^f)^H \left(\frac{1}{J} \sum_{l=1}^J \mathbf{T}(w_l) \mathbf{T}^H(w_l) \right) \mathbf{w}_\theta^f \quad (47)$$

where we assumed for simplicity that the noise spectrum is frequency independent, i.e., $\sigma_n^2(w) = \sigma_n^2$, and \mathbf{w}_θ^f is defined by (10). Limiting the white noise gain yields the following quadratic constraint

$$(\mathbf{w}_\theta^f)^H \mathbf{Q} \mathbf{w}_\theta^f \leq T_0 \quad (48)$$

where

$$\mathbf{Q} \triangleq \frac{1}{J} \sum_{l=1}^J \mathbf{T}(w_l) \mathbf{T}^H(w_l) \quad (49)$$

and T_0 is a design parameter. Note, that for the case of unitary focusing transformations, \mathbf{Q} is reduced to the unit matrix and the lower bound for T_0 reduces to the white noise gain of the conventional beamformer. We can see from (47) that in the general case the focusing transformations lead to spatially non-white noise. As the noise covariance is known up to a positive scaling factor, then one may apply a prewhitening transformation, e.g., [1], and proceed with the conventional diagonal loading technique. Equivalently, one can verify that the robust focused MVDR weight vector satisfying (48) is given by

$$\mathbf{w}_\theta^{f,QL} = \frac{(\mathbf{R}_x^f + \beta \mathbf{Q})^{-1} \mathbf{a}_\theta(w_0)}{\mathbf{a}_\theta^H(w_0) (\mathbf{R}_x^f + \beta \mathbf{Q})^{-1} \mathbf{a}_\theta(w_0)} \quad (50)$$

where β is the Lagrange multiplier which is determined so that the quadratic constraint (48) is satisfied. Since (48) is a monotonic decreasing function of β , any iterative scheme may be used

to find β [1]. Note that in (50) the loading term $\beta \mathbf{Q}$ is a non-diagonal matrix, thus, for the focused MVDR case we use the notation Q-loading.

In Sections VII–IX, we conduct a numerical performance analysis of the AG of the Q-loaded MVDR focused beamformer based on Monte Carlo simulations and the asymptotic expression (61) (see the Appendix). We compare the analytic AG to the simulative AG based on Monte Carlo runs of the SMI implementation. We compare the performance of various focusing methods and study their dependence on the accuracy of the focusing transformation.

VII. NUMERICAL STUDY FOR THE CASE OF DOAS UNCERTAINTIES

In this section, we conduct a numerical study of the focusing errors and of the AG of the Q-loaded MVDR focused beamformer in the presence of DOAs uncertainties. We compare the performance of three focusing transformations: BFT representing the Bayesian focusing approach, WINGS representing the panoramic focusing approach and the Wang–Kaveh Focusing Transformation (WKFT) [13] representing the directional focusing approach, which focuses a discrete set of preliminary DOA estimates. We evaluate the analytic AG given by (61) and compare it to the simulative AG based on Monte Carlo simulations of the MVDR-SMI focused beamformer. In our first example, we take two circular complex Gaussian wideband acoustic sources propagating towards a linear array of $N = 20$ sensors in velocity of 1500 m/s. The simulation results were obtained by averaging over 100 independent Monte Carlo runs. We simulate the actual DOA errors as Gaussian random variables with a standard deviation on the order of half the 3 dB beamwidth. The mean DOAs vector is $\boldsymbol{\theta} = [70^\circ, 105^\circ]$, where 90° is the broadside direction, and the desired signal is the one arriving from 105° . The signal-to-interference ratio (SIR) is set at a fixed value of -20 dB. The bandwidth of the sources is 600 Hz taken around $f_c = 1500$ Hz and the spectrum is taken to be flat in the relevant bandwidth. The sampling frequency is 4800 Hz and the focusing frequency is $f_0 = 1500$ Hz. The observation time T is taken as 10 seconds and divided into $K = 46$ snapshots. Each snapshot of data is transformed to the frequency domain using an FFT of 1024 bins yielding $J = 129$ frequency bins in the relevant bandwidth. The spacing between two adjacent sensors is $d = \lambda_{\min}/2$, where λ_{\min} corresponds to the highest frequency of the bandwidth. Note that in array processing applications $D/c \ll 1/B$ should be used (see, e.g., [35]) to determine whether the narrowband assumption can be applied, where D is the array length, c is the signal velocity and B is the signal bandwidth. The parameters used in our examples indicate wideband scenario. For the BFT, we take the weighting function $\rho^2(\theta)$ (13), to be a sum of Gaussian densities centered around the presumed DOAs

$$\rho^2(\theta) = \frac{1}{\sqrt{2\pi\sigma_1^2}} \exp\left(-\frac{(\theta - \theta_1)^2}{2\sigma_1^2}\right) + \frac{1}{\sqrt{2\pi\sigma_2^2}} \exp\left(-\frac{(\theta - \theta_2)^2}{2\sigma_2^2}\right) \quad (51)$$

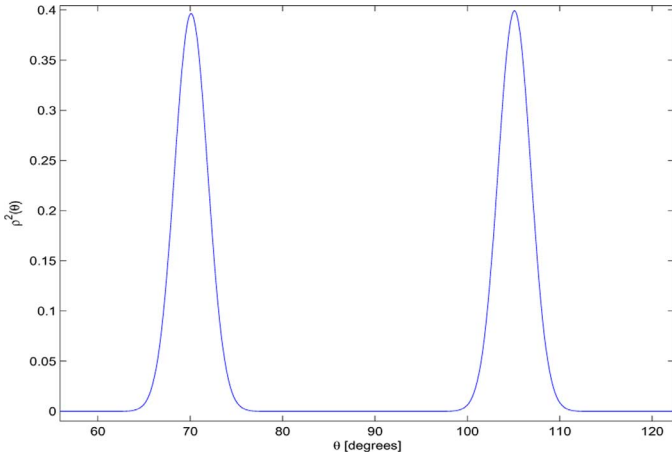


Fig. 2. Weighting function $\rho^2(\theta)$ taken for the BFT.

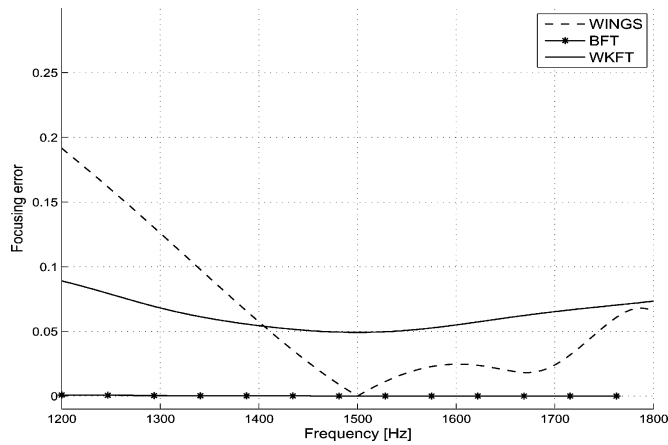


Fig. 3. Squared focusing transformation error versus frequency for BFT, WINGS, and WKFT for the case of two sources and DOAs uncertainties.

where θ_1 and θ_2 are the presumed DOAs of the sources. $\sigma_1 = 1.27$ and $\sigma_2 = 1.25$ are the standard deviations, approximately on the order of a quarter of the 3-dB beamwidth of the array at θ_1 and θ_2 , respectively. Fig. 2 illustrates the weighting function, $\rho^2(\theta)$, taken for the BFT. In the WKFT method we add 2 auxiliary directions for each assumed DOA in order to increase the robustness to DOAs uncertainties. The auxiliary directions were added at a quarter of the 3-dB beamwidth from the presumed DOAs.

In order to compute the BFT transformation in the angular domain as discussed in Section V, we sample the steering matrix $\hat{\mathbf{A}}_L^p(w)$ (37a) at $L = 2n_\epsilon + n_\rho = 3k_{\max}r_{\max} + n_\rho$ points. We take $n_\rho = 259$ since the Fourier coefficients of $\rho(\theta)$ beyond this value have magnitude smaller than $1e - 6$. Thus, $n_\epsilon = 32$, and $L = 355$. Since the LS fit may be performed only in sectors around the presumed DOAs, we actually took only $\tilde{L} = 22$ points covering two sectors of 10 degrees each.

Let us first examine the focusing errors for the various focusing methods. Fig. 3 shows the squared focusing error $\|\mathbf{e}_\theta(w_j)\|^2$ (21) versus frequency, averaged over 100 Monte Carlo runs and summed over all the true source directions, for the BFT, WINGS, and WKFT methods. It can be seen that the BFT method has the lowest focusing error along the entire bandwidth. In the WINGS method, we see that large errors occur at frequencies below the focusing frequency. This

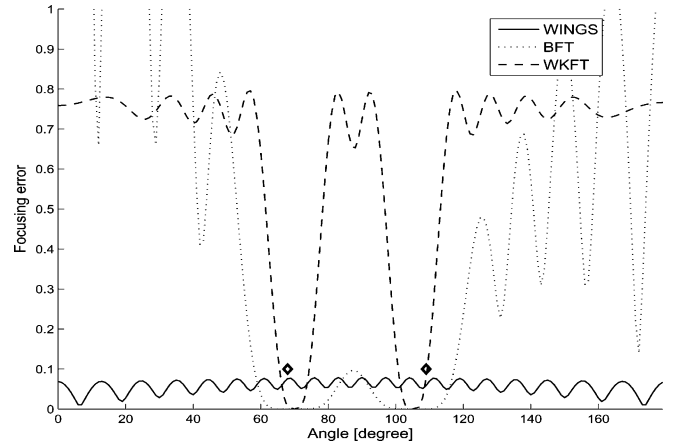


Fig. 4. Squared focusing error versus angle due to focusing from $f = 1350$ Hz to $f_0 = 1500$ Hz for BFT, WINGS, and WKFT, for the case of two sources and DOAs uncertainties.

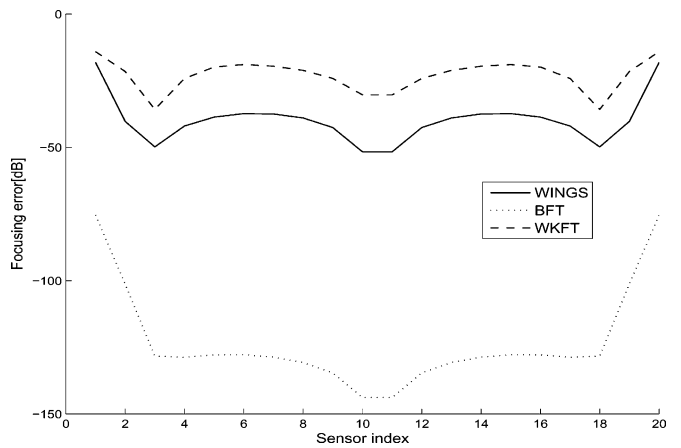


Fig. 5. Average squared focusing error in the desired source direction versus sensor index for BFT, WINGS, and WKFT for the case of two sources and DOA uncertainties.

is expected since WINGS is an interpolation based focusing method, in which focusing is equivalent to spatial interpolation [22] of the array. Interpolating from a low frequency to a higher one, is equivalent to extrapolating the array beyond its physical length, thus, yielding high focusing errors. One can reduce the WINGS transformation error by focusing to the lowest frequency of the bandwidth. However, this will reduce the effective aperture of the focused array, thus reducing the spatial resolution of the array. In the literature there are several papers dealing with the issue of choosing the optimal focusing frequency (e.g., [36], [37]).

Fig. 4 shows the squared focusing error versus azimuth at $f = 1350$ Hz for the BFT, WINGS, and WKFT methods with DOA errors of approximately 3 degrees for each source. The true DOAs are marked by diamonds. It can be seen that the WINGS method has a roughly equi-ripple focusing error for all the directions. This is expected because WINGS is an interpolated based focusing method which does not depends on the DOAs. Both BFT and WKFT have a high focusing error far from the assumed DOAs, and a low focusing error close to the assumed DOAs. It can be seen that BFT is significantly more robust to DOA uncertainties since they have a low focusing error over a wider range of angles.

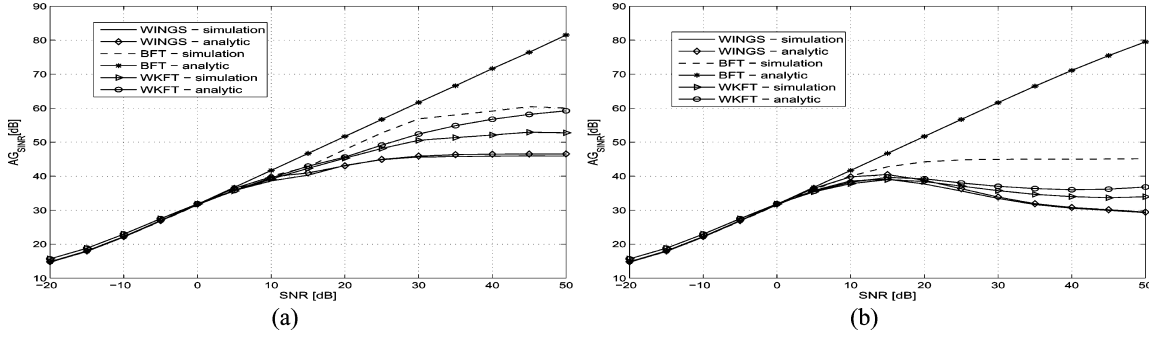


Fig. 6. Array gain versus SNR for BFT, WINGS, and WKFT for the case of two sources with DOA uncertainties. (a) With Q-loading, and (b) without Q-loading.

Fig. 5 shows the focusing error for each element along the array in the desired source direction, averaged over the entire bandwidth, for the BFT, WINGS, and WKFT focusing methods, for a DOA error of approximately 3 degrees. We can see that BFT has the smallest focusing error along the array while WKFT has the largest errors. We can also see that the error of the BFT and WINGS methods increases significantly towards the edges of the array. This increase is due to the fact that both methods are based on spatial interpolation of the array, which requires extrapolating the array beyond its physical length, thus causing increasing errors at the edges of the array.

Let us now evaluate the performance of the Q-loaded SMI-MVDR beamformer for the various focusing schemes. For Q-loading, we set the quadratic constraint value at $T_0 = 0.25$ which is five times the norm of the conventional beamformer. In Fig. 6(a) and (b), we plot the asymptotic and the simulative AG versus SNR for BFT, WINGS, and WKFT focusing for the coherent MVDR with and without Q-loading, respectively. The superior performance of the BFT over that of the WINGS and WKFT in both analytic and simulative curves, is expected due to its low focusing error. The performance difference is very large in the analytic AG curves and increases with SNR; however, the simulative curves exhibit a smaller yet still significant performance difference. We note that the difference between the analytic and simulative AG is due to the fact that the analytic calculation uses the asymptotic focused covariance matrix (53) while the simulation uses its estimated sample covariance matrix (9) averaged over $K = 46$ snapshots.

Comparing Fig. 6(a) and (b) we can observe the improvement of the AG due to Q-loading of the covariance matrix. We see that the Q-loading effectively reduces the sensitivity of the MVDR beamformer to the focusing errors of the various methods as well as to the SMI estimation errors and DOA uncertainties. In Fig. 7, the AG versus ISR is plotted for an SNR value of 40 dB, we see that the BFT exhibits superior performance for all SIR values.

Let us now examine a single source example. In Fig. 8(a) and (b), we plot the asymptotic and the simulative AG versus SNR for BFT, WINGS, and WKFT methods for the single-source case with DOA uncertainties for the MVDR focused beamformer with and without Q-loading, respectively. First, we note the significant improvement in the AG achieved by the Q-loading. Without Q-loading the AG decreases to

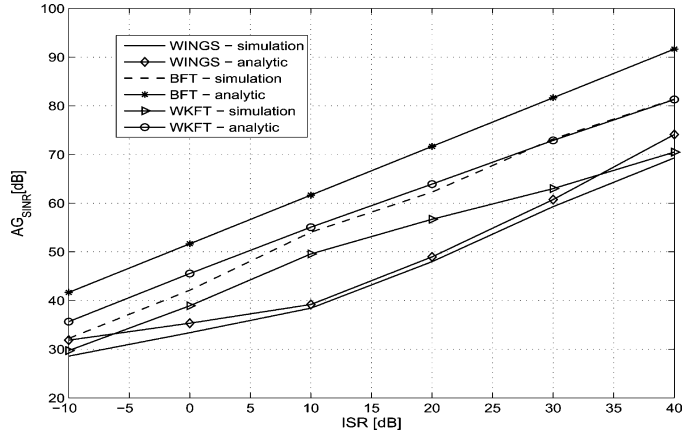


Fig. 7. Array gain versus ISR for SNR = 40 dB, two sources with DOA uncertainties and using Q-loading.

values below -40 dB, while with Q-loading we observe a slight decrease in the AG for mid range SNR values. However, as the SNR increases the Q-loading term becomes significant and the AG converges to a steady value, which depends on the focusing errors. The comparison of the performance of the different focussing methods for the single-source case given in Fig. 8 shows a significant advantage of the BFT over that of WINGS; however, the WKFT exhibits superior performance than both BFT and WINGS. We see in the low and mid SNR range that WKFT has a moderate advantage over the BFT in the simulative curve. From both Fig. 8(a) and (b), it can be seen that WKFT achieves an AG about 1 dB higher than that of the BFT in the region of the low SNR values. The reason for this is that in both BFT and WINGS, the beamwidth is wider than that of the WKFT as can be seen in Fig. 9(a) where the beampatterns of all the methods are plotted for the single-source case and for a low SNR value of -10 dB. To understand this phenomena, we examine in Fig. 9(b) the corresponding magnitudes of the adaptive coefficients vector. In BFT and WINGS which are considered to be interpolation based methods, it can be seen that the “effective” array is reduced to only 16 sensors while the physical array was 20 sensors. Since the single source AG is roughly $10 \log_{10} N$, we get a difference of approximately 1 dB in the AG. This reduction in the AG decreases as the relative processed bandwidth is decreased.

The results presented in this section demonstrated a significant performance improvement of the BFT over the WINGS and

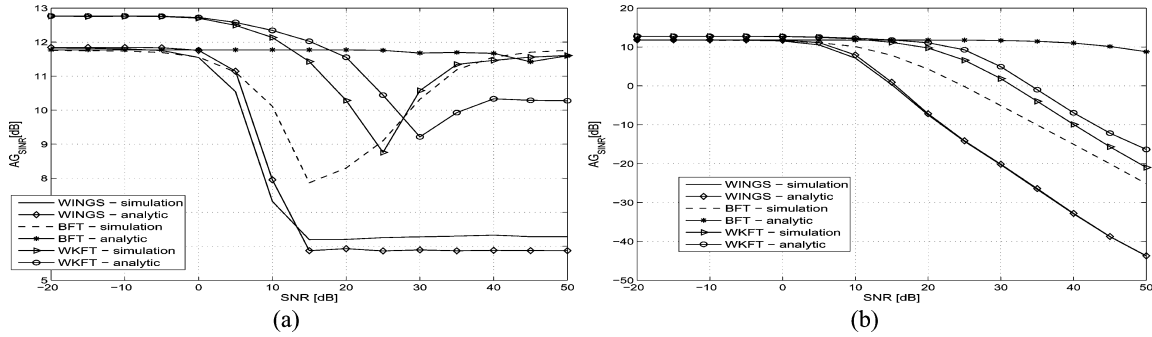


Fig. 8. Array gain versus SNR for BFT, WINGS, and WKFT, for the single-source case with DOA uncertainty. (a) With Q-loading, and (b) without Q-loading.

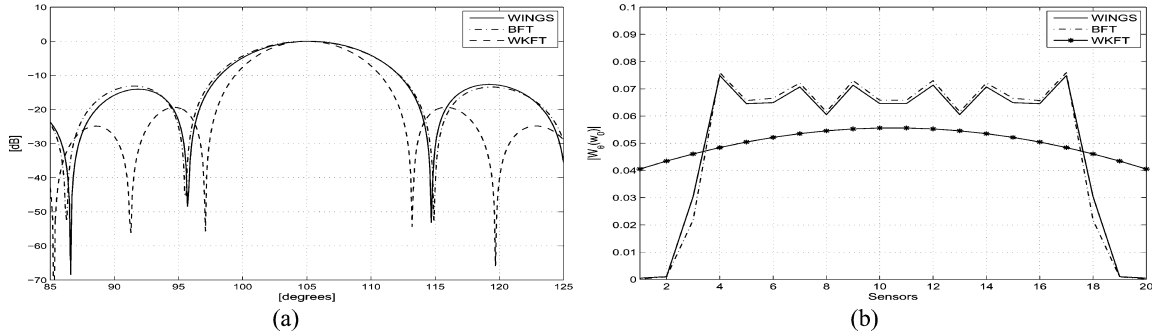


Fig. 9. (a) Beampattern versus angle for the various methods for the single-source case and $SNR = -10$ dB. (b) Norm of the MVDR coefficients versus sensors for the various methods for the single-source case and $SNR = -10$ dB.

WKFT focusing methods in multisource scenarios with DOAs uncertainties. However, in the single-source case, WKFT exhibits better performance than that of the BFT and WINGS, since panoramic focusing methods based on spatial interpolation tend to have a wider beamwidth which reduces the AG. This appears to be a tradeoff between the panoramic and the directional focusing approaches. However, the AG loss is moderate and it reduces as the relative bandwidth is decreased. We also showed the effectiveness of Q-loading introduced in Section VI in improving the robustness of the focused MVDR beamformer in handling focusing errors and SMI implementation errors.

An eminent point arising from Figs. 6(b) and 8(b) is the degradation in the performance of the focused MVDR as the SNR increases. In Section VIII, we investigate this degradation further showing that it occurs mainly due to the focusing error in the desired source direction, we also examine the quality of approximation (46) by comparing it to the analytic AG (61).

VIII. SENSITIVITY OF FOCUSED UNLOADED MVDR BEAMFORMER TO TRANSFORMATION ACCURACY

In this section, we investigate the sensitivity of the focused MVDR to focusing errors. We will concentrate on the single-source case whose DOA is assumed to be known perfectly, and we will also compare the sensitivity predicted by approximation (46) to that of the analytic AG (61).

Fig. 10 shows the analytic and simulative AG versus SNR of WINGS, and BFT, for the single-source case with perfect knowledge of the DOA without Q-loading. The source DOA is taken to be $\theta = 105^\circ$. The simulative curves are very similar to those of the previous section. The BFT method achieves better performance due to its low focusing error; however, its simulative AG decreases at high SNR. We observe that the analytic and

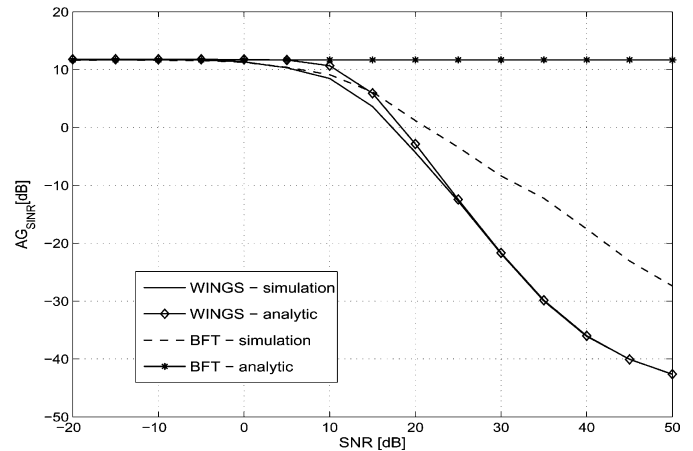


Fig. 10. Simulative and analytic array gain versus SNR, for the WINGS and BFT methods, for the single-source case with perfect knowledge of the DOA, without Q-loading.

simulative performance of WINGS is severely degraded at high SNR values. The fact that the degradation in the single-source case is very similar to that of the multi-source case indicates that the performance is mainly sensitive to the focusing errors in the desired source DOA, and less sensitive to the focusing errors in the interferences DOAs.

In Section VI, we developed an analytic expression to the approximated AG (46) for a single source with a single frequency which indicates that the output AG is inversely proportional to ξ^2 for $\xi \gg 1$. Figs. 11(a) and 12(a) compare the analytic (61) and approximated (46) AG of the BFT and WINGS methods for the case of single frequency focusing. Fig. 11(a) shows the case of downward focusing from $f = 1710$ Hz to a lower frequency $f_0 = 1500$ Hz, and Fig. 12(a) shows the case of upward focusing

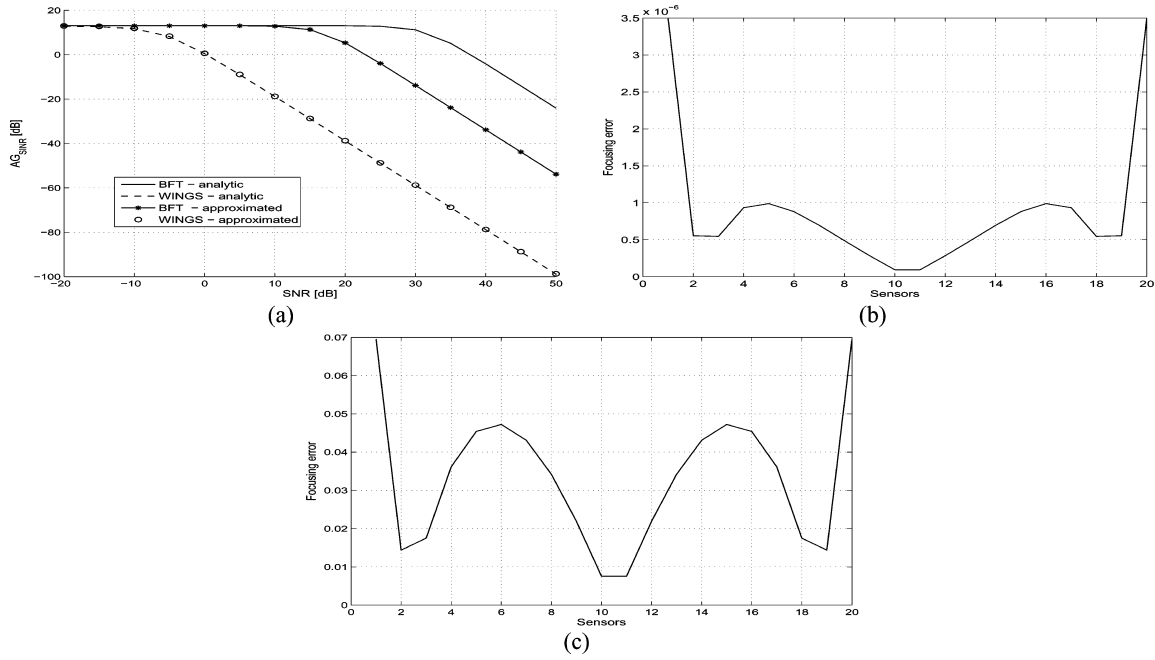


Fig. 11. (a) Analytic AG (61) for BFT (solid) and WINGS (dashed), and the approximated AG (46) for BFT (stars) and WINGS (circles) for the case of a single frequency $f_j = 1710$ Hz transformed to the focusing frequency $f_0 = 1500$ Hz. (b) Squared focusing error of BFT versus sensor index. (c) Squared focusing error of WINGS versus sensor index.

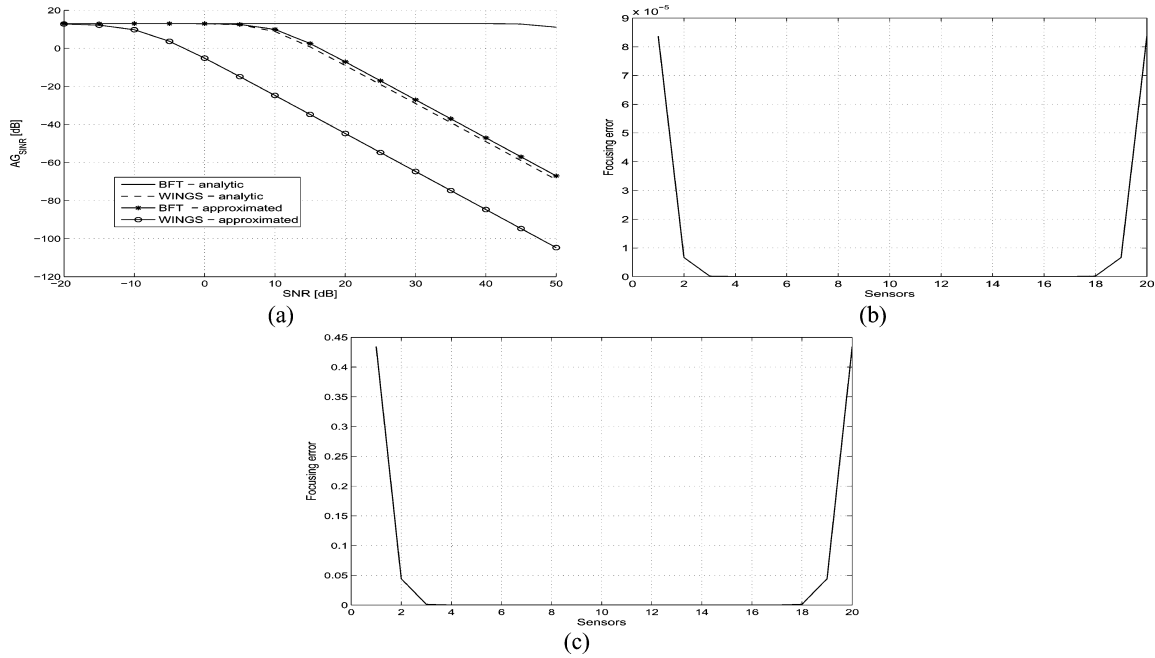


Fig. 12. (a) Analytic AG (61) for BFT (solid), and for WINGS (dashed), the approximated AG (46) for BFT (stars) and for WINGS (circles) for the case of a single frequency $f_j = 1240$ Hz transformed to the focusing frequency of $f_0 = 1500$ Hz. (b) Squared focusing error of BFT versus sensor index. (c) Squared focusing error of WINGS versus sensor index.

from $f = 1240$ Hz to $f_0 = 1500$ Hz. Figs. 11(b) and (c) and 12(b) and (c) plot the corresponding focusing errors. We can see from Fig. 11(a) that for downward focusing, we get a relatively good fit of the analytic (61) and the approximated (46) AG, especially in the WINGS method. The AG begin decreasing at a rate of $1/\xi^2$ from $\xi \approx 20$ dB for the BFT and from $\xi \approx -10$ dB for the WINGS. The relatively small and roughly uniform error in Fig. 11(b) and (c) justifies the good fit of (46) and (61) in this case. In Fig. 12(a), we see a significant difference between the analytic and approximated AG for upward focusing. This is

due to the highly non uniform distribution of the focusing errors across the array for both BFT and WINGS methods, as illustrated in Fig. 12(b) and (c). In this case the statistical model assumptions are not valid and the approximated AG (46) may not be used. However we note that also in this case we observe a rate decay of $1/\xi^2$ in the WINGS as predicted by (46).

From both Figs. 6(a) and 8(a) it can be seen that the Q-loaded focused beamformer achieves a superior performance over that of the unloaded focused beamformer, yet, performance degradation is still exist in the Q-loaded case. In [38], we propose an

alternative robust method for focused wideband MVDR beamforming. The proposed method is based on the general-rank MVDR [39] which bring into account the focusing transformations in the optimization function, thus effectively reducing the sensitivity of the MVDR to focusing errors. Simulation results in [38] demonstrated an additional improvement with respect to the Q-loaded focused MVDR beamformer.

IX. CONCLUSION

We proposed and investigated a Bayesian approach for focusing transformation design, which takes into account the statistical uncertainties in the DOAs during the focusing process. The Bayesian focusing approach is a compromise between the directional focusing approach which requires *a priori* knowledge of the DOAs, and the panoramic focusing approach which employs spatial interpolation in order to focus all directions. The solution to the Bayesian focusing problem yields an optimal MMSE focusing transformation and consequently an improved focused beamformer with better AG. We derived a closed-form expression for the BFT based on the weighted WINGS focusing transformation and provide an extension for directional sensors and empirically calibrated arrays. We examined the use of a simple and computationally efficient LS approximation in the angle domain and derived an angular sampling condition. We proved that the angle domain approximation is identical to the optimal BFT if the sampling condition is satisfied. We note that the angular sampling condition is derived from the wavefield modeling representation of the array and depends on the maximal spatial frequency component $k_{\max}r_{\max}$ for an array in free field.

We studied the sensitivity of the focused beamformer to focusing errors, especially at high SNR values. We analyzed this sensitivity and derived an analytic approximated expression for the AG as a function of the input SNR ξ and the focusing errors which are approximated as random errors across the array with a given variance. We showed that, under this assumption, the AG is approximately inversely proportional to ξ^2 for $\xi \gg 1$ and inversely proportional to $\sigma_g^2(1+\sigma_g^2)$ for $N \gg 1$ and $N \gg \sigma_g^2 > 0$. We also showed that the high sensitivity of the focused beamformer to focusing errors mainly results from the focusing errors in the desired source direction.

We treated the important issue of reducing the beamformers' sensitivity to focusing errors, and other modeling errors. We extended the narrowband diagonal loading scheme to a generalized Q-loading scheme for the focused wideband MVDR beamformer, which employs a generalized *transformation-dependent* loading of the covariance matrix, thus taking into account the focusing process. We note that the Q-loaded MVDR beamformer is a *transformation-dependent* process, which may be applied after any arbitrary focusing scheme for robust focused beamforming. In the numerical section we demonstrated the significant improvement in the robustness of the focused MVDR beamformer due to Q-loading.

To evaluate the performance of the proposed BFT method and several other focusing methods we derived an analytic expression of the asymptotic AG for the SMI-implementation of the focused Q-loaded MVDR beamformer. Simulation results

have illustrated the superiority of the proposed BFT method, for the multisource case with DOA uncertainties, over that of the WINGS and WKFT focusing methods. This improvement is attributed to the low focusing error of the BFT across the entire bandwidth, which yields more accurate focused data. However, in the single-source case, WKFT exhibits better performance than that of the BFT and WINGS, since panoramic focusing methods based on spatial interpolation tend to have a wider beamwidth which moderately reduces the AG. The AG loss is expected to decrease as the relative bandwidth is decreased.

APPENDIX

ANALYTIC ARRAY GAIN OF THE MVDR FOCUSED BEAMFORMER

In this appendix, we derive an analytic expression for the AG of the Q-loaded MVDR focused beamformer (50) as a function of the focusing transformations. The focusing process introduces a frequency dependent transformation error which affects the performance of the MVDR focused beamformer. The analytic AG will be used to evaluate the performance of the focused beamformer for the various focusing methods. The expression developed here is the asymptotic limit to the performance since it involves the asymptotic covariance matrix of the data. The model assumptions are specified in Section II. For the sake of simplicity we also assume that the sources are uncorrelated and that the desired source direction is known. The covariance matrix of the received focused data vector $\mathbf{y}_k(n)$ (6) is given by

$$\begin{aligned} \mathbf{R}_x^f &= E \{ \mathbf{y}_k(n) \mathbf{y}_k^H(n) \} \\ &= E \left\{ \sum_{j,l=1}^J \mathbf{T}(w_j) \mathbf{x}_k(w_j) e^{i w_j n T_s} \right. \\ &\quad \left. \times (\mathbf{T}(w_l) \mathbf{x}_k(w_l) e^{i w_l n T_s})^H \right\}. \end{aligned} \quad (52)$$

For a large enough observation interval, different frequencies become statistically independent, and (52) becomes

$$\begin{aligned} \mathbf{R}_x^f &= \sum_{j=1}^J \mathbf{T}(w_j) E \{ \mathbf{x}_k(w_j) \mathbf{x}_k^H(w_j) \} \mathbf{T}^H(w_j) \\ &\triangleq \sum_{j=1}^J \mathbf{T}(w_j) \mathbf{R}_x(w_j) \mathbf{T}^H(w_j). \end{aligned} \quad (53)$$

Let $s_1(t)$ be the desired signal propagating from θ_1 , let P_{s_1}, P_i, P_n be the power of the desired signal, the interferences signals, and the noise, respectively, then

$$\begin{aligned} P_{s_1} &= \sum_{j=1}^J \sigma_{s_1}^2(w_j) \\ P_i &= \sum_{p=2}^P \sum_{j=1}^J \sigma_{s_p}^2(w_j) \\ P_n &= \sum_{j=1}^J \sigma_n^2(w_j) \end{aligned} \quad (54)$$

$$AG = \frac{\mathbf{a}_{\theta_1}^H(w_0)(\tilde{\mathbf{R}}_x^f)^{-1} \left(\sum_{j=1}^J \sigma_{s_1}^2(w_j) \mathbf{a}_{\theta_1}^f(w_j) (\mathbf{a}_{\theta_1}^f(w_j))^H \right) (\tilde{\mathbf{R}}_x^f)^{-1} \mathbf{a}_{\theta_1}(w_0)}{\mathbf{a}_{\theta_1}^H(w_0)(\tilde{\mathbf{R}}_x^f)^{-1} \left(\sum_{j=1}^J \left[\sum_{p=2}^P \sigma_{s_p}^2(w_j) \mathbf{a}_{\theta_p}^f(w_j) (\mathbf{a}_{\theta_p}^f(w_j))^H + \mathbf{R}_n^f(w_j) \right] \right) (\tilde{\mathbf{R}}_x^f)^{-1} \mathbf{a}_{\theta_1}(w_0) \cdot \text{SINR}_{\text{in}}} \quad (61)$$

where $\sigma_{s_p}^2(w_j)$, $p = 1, 2, \dots, P$ is the power density of the p th source at frequency w_j . Let us define

$$\mathbf{a}_{\theta}^f(w_j) = \mathbf{T}(w_j) \mathbf{a}_{\theta}(w_j) \quad (55)$$

to be the focused steering vector in direction θ and frequency w_j .

Let also $P_{s_1\text{-out}}$, $P_{i\text{-out}}$, $P_{n\text{-out}}$ denote the output power of the desired signal, the interferences, and the noise, respectively, then one can see that

$$P_{s_1\text{-out}} = \sum_{j=1}^J \sigma_{s_1}^2(w_j) \left| \left(\mathbf{w}_{\theta_1}^{f,QL} \right)^H \mathbf{a}_{\theta_1}^f(w_j) \right|^2 \quad (56)$$

$$P_{i\text{-out}} = \sum_{p=2}^P \sum_{j=1}^J \sigma_{s_p}^2(w_j) \left| \left(\mathbf{w}_{\theta_1}^{f,QL} \right)^H \mathbf{a}_{\theta_p}^f(w_j) \right|^2 \quad (57)$$

$$P_{n\text{-out}} = \left(\mathbf{w}_{\theta_1}^{f,QL} \right)^H \times \left(\sum_{j=1}^J \sigma_n^2(w_j) \mathbf{T}(w_j) \mathbf{T}^H(w_j) \right) \mathbf{w}_{\theta_1}^{f,QL} \quad (58)$$

where $\mathbf{w}_{\theta_1}^{f,QL}$ is the Q-loaded focused MVDR weight vector at direction θ_1

$$\mathbf{w}_{\theta_1}^{f,QL} = \frac{(\mathbf{R}_x^f + \beta \mathbf{Q})^{-1} \mathbf{a}_{\theta_1}(w_0)}{\mathbf{a}_{\theta_1}^H(w_0) (\mathbf{R}_x^f + \beta \mathbf{Q})^{-1} \mathbf{a}_{\theta_1}(w_0)}. \quad (59)$$

Defining the SINR_{in} , SINR_{out} to be the signal-to-interference-plus-noise ratio (SINR) at the input and output of the beamformer, respectively

$$\begin{aligned} \text{SINR}_{\text{in}} &= \frac{P_{s_1}}{P_i + P_n} \\ \text{SINR}_{\text{out}} &= \frac{P_{s_1\text{-out}}}{P_{i\text{-out}} + P_{n\text{-out}}} \end{aligned} \quad (60)$$

then, the AG is the ratio between SINR_{out} and SINR_{in} . Substituting (59) into (56)–(58), yields (61), shown at the top of the page, where

$$\tilde{\mathbf{R}}_x^f = \mathbf{R}_x^f + \beta \mathbf{Q} \quad (62)$$

and

$$\mathbf{R}_n^f(w_j) = \sigma_n^2(w_j) \mathbf{T}(w_j) \mathbf{T}^H(w_j) \quad (63)$$

is the focused noise covariance matrix.

In order to calculate \mathbf{R}_x^f using (53), $\mathbf{R}_x(w_j)$ should be evaluated as

$$\mathbf{R}_x(w_j) = \sum_{p=1}^P \sigma_{s_p}^2(w_j) \mathbf{a}_{\theta_p}(w_0) \mathbf{a}_{\theta_p}^H(w_0) + \sigma_n^2(w_j) \mathbf{I}. \quad (64)$$

REFERENCES

- [1] H. L. Van-trees, *Detection, Estimation and Modulation Theory, Part IV—Optimum Array Processing*. New York: Wiley Interscience, 2002.
- [2] T. S. Rappaport, *Smart Antennas*. New York: IEEE Press, 1998.
- [3] A. J. Paulraj and C. B. Papadias, “Space-time processing for wireless communications,” *IEEE Signal Process.*, vol. 14, no. 6, pp. 49–78, Nov. 1997.
- [4] T. Do-Hong and P. Russer, “Signal processing for wideband smart antenna array applications,” *IEEE Microw. Mag.*, vol. 5, no. 1, pp. 57–67, Mar. 2004.
- [5] S. Ohmori, Y. Yamao, and N. Nakajima, “The future generations of mobile communications based on broadband access technologies,” *IEEE Commun Mag.*, vol. 38, no. 12, pp. 134–142, Dec. 2000.
- [6] S. Haykin, *Adaptive Filters Theory*, 4th ed. Englewood Cliffs, NJ: Prentice-Hall, 1996.
- [7] W. Liu and R. J. Langley, “An adaptive wideband beamforming structure with combined subband decomposition,” *IEEE Trans. Antennas Propag.*, vol. 57, no. 7, pp. 2204–2207, Jul. 2009.
- [8] R. P. Gooch and J. J. Shynk, “Wide-band adaptive array processing using zero-pole digital filters,” *IEEE Trans. Antennas Propag.*, vol. 34, no. 3, pp. 355–367, Mar. 1986.
- [9] H. Hung and M. Kaveh, “Focusing matrices for coherent signal subspace processing,” *IEEE Trans. Acoust. Speech Signal Process.*, vol. 36, no. 8, pp. 1272–1281, Aug. 1988.
- [10] S. Simanpalli and M. Kaveh, “Broadband focusing for partially adaptive beamforming,” *IEEE Trans. Aerosp. Electron. Syst.*, vol. 30, no. 1, pp. 68–80, Jan. 1994.
- [11] J. F. Wang and M. Kaveh, “Coherent signal-subspace transformation beamformer,” *IEE Proc., Pt. F*, vol. 137, no. 4, pp. 267–275, Aug. 1990.
- [12] M. A. Doron and A. Nevet, “Robust wavefield interpolation for adaptive wideband beamforming,” *Signal Process.*, vol. 80, pp. 1579–1594, 2008.
- [13] H. Wang and M. Kaveh, “Coherent signal subspace processing for the detection and estimation of angles of multiple wide band sources,” *IEEE Trans. Acoust., Speech, Signal Process.*, vol. ASSP-33, no. 4, pp. 823–831, Aug. 1985.
- [14] M. A. Doron and A. J. Weiss, “On focusing matrices for wideband array processing,” *IEEE Trans. Signal Process.*, vol. 40, no. 6, pp. 1295–1302, Jun. 1992.
- [15] M. A. Doron, E. Doron, and A. J. Weiss, “Coherent wide-band processing for arbitrary array geometry,” *IEEE Trans. Signal Process.*, vol. 41, no. 1, pp. 414–417, Jan. 1993.
- [16] T. Do-Hong, F. Demmel, and P. Russer, “Wideband direction-of-arrival estimation using frequency-domain frequency-invariant beamformers: An analysis of performance,” *IEEE Microw. Wireless Compon. Lett.*, vol. 14, no. 8, pp. 383–385, Aug. 2004.
- [17] F. Sellone, “Robust auto-focusing wideband DOA estimation,” *Signal Process.*, vol. 86, pp. 17–37, 2006.
- [18] B. Friedlander and A. J. Weiss, “Direction finding for wide-band signals using an interpolated array,” *IEEE Trans. Signal Process.*, vol. 41, no. 4, pp. 1618–1634, Apr. 1993.

- [19] E. D. D. Claudio, "Robust ML wideband beamforming in reverberant fields," *IEEE Trans. Signal Process.*, vol. 51, no. 2, pp. 338–349, Feb. 2003.
- [20] J. Wang, Q. Feng, R. Wu, and Z. Su, "A constant-beamwidth beamforming method for acoustic imaging," in *Proc. Antennas Propag. Int. Symp.*, 2007.
- [21] Y. H. Chen and F. P. Yu, "Broadband adaptive beamforming based on coherent signal subspace using spatial interpolation preprocessing," *Radar Signal Process., IEE Proc. F*, vol. 138, no. 5, pp. 489–494, Oct. 1991.
- [22] J. Krolik and D. Swingler, "Focused wide-band array processing by spatial resampling," *IEEE Trans. Acoust. Speech Signal Process.*, vol. 38, no. 2, pp. 356–360, Feb. 1990.
- [23] M. A. Doron and E. Doron, "Wavefield modeling and array processing; part I—Spatial sampling," *IEEE Trans. Signal Process.*, vol. 42, no. 10, pp. 2549–2559, Oct. 1994.
- [24] T. Yu and J. H. L. Hansen, "Robust auto-focusing wideband Bayesian beamforming," in *Proc. 2nd Joint Workshop Hands-Free Speech Commun. Microphone Arrays, HSCMA'08*, Trento, Italy, 2008, pp. 61–64.
- [25] J. Capon, "High resolution frequency-wavenumber spectrum analysis," *Proc. IEEE*, vol. 57, no. 8, pp. 1408–1418, Aug. 1969.
- [26] H. Cox, "Resolving power and sensitivity to mismatch of optimum array processors," *J. Acoust. Soc. Amer.*, vol. 54, no. 3, pp. 771–785, 1973.
- [27] B. D. Carlson, "Covariance matrix estimation errors and diagonal loading in adaptive arrays," *IEEE Trans. Aerosp. Electron. Syst.*, vol. 24, no. 4, pp. 397–401, Jul. 1988.
- [28] Y. Bucris, I. Cohen, and M. A. Doron, "Bayesian focusing transformation for coherent wideband array processing," in *Proc. 25th IEEE Conv. Elect. Electron. Eng. in Israel, IEEEI-2008*, Eilat, Israel, Dec. 3–5, 2008, pp. 479–483.
- [29] M. Abramowitz and I. A. Stegun, *Handbook of Mathematical Functions*. New York: Dover, 1970.
- [30] A. V. Oppenheim and R. W. Schaffer, *Discrete-Time Signal Processing*. Englewood Cliffs, NJ: Prentice-Hall, 1989.
- [31] W. S. Youn and C. K. Un, "Robust adaptive beamforming based on the eigenstructure method," *IEEE Trans. Signal Process.*, vol. 42, no. 6, pp. 1543–1547, Jun. 1994.
- [32] H. Cox, R. M. Zeskind, and M. M. Owen, "Robust adaptive beamforming," *IEEE Trans. Acoust., Speech, Signal Process.*, vol. 35, no. 10, pp. 1365–1376, Oct. 1987.
- [33] C. C. Lee and J. H. Lee, "Robust adaptive array beamforming under steering vectors errors," *IEEE Trans. Antennas Propag.*, vol. 45, no. 1, pp. 168–175, Jan. 1997.
- [34] J. Li and P. Stoiche, *Robust Adaptive Beamforming*. Hoboken, NJ: Wiley Interscience, 2006.
- [35] R. T. Compton, *Adaptive Antennas: Concept and Performance*. Englewood Cliffs, NJ: Prentice-Hall, 1988.
- [36] S. Valaee and P. Kabel, "The optimal focusing subspace for coherent signal subspace processing," *IEEE Trans. Signal Process.*, vol. 44, no. 3, pp. 752–756, Mar. 1996.
- [37] D. Swingler, P. Kabel, and J. Huang, "Source location bias in the coherently focused high—Resolution broad band beamformer," *IEEE Trans. Acoust. Speech, Signal Process.*, vol. 37, no. 1, pp. 143–145, Jan. 1989.
- [38] Y. Bucris, I. Cohen, and M. A. Doron, "Robust focusing for wideband MVDR beamforming," in *Proc. 6th IEEE Sens. Array Multichannel Signal Process. Workshop*, Israel, Oct. 4–7, 2010, pp. 1–4.
- [39] S. Shahbazpanahi, A. B. Gershman, Z. Luo, and K. M. Wong, "Robust adaptive beamforming for general-rank signal models," *IEEE Trans. Signal Process.*, vol. 9, no. 9, pp. 2257–2269, Sep. 2003.



Yaakov Bucris (S'08) received the B.Sc. and M.Sc. degrees in electrical engineering from the Technion—Israel Institute of Technology, Haifa, in 2005 and 2011, respectively.

Since 2002 he has been with RAFAEL, Advanced Defence Systems Ltd, Haifa, Israel, as a Research Engineer in the underwater acoustic communication group. Since 2005, he has also been a Teaching Assistant and a Project Supervisor with the Communications Lab, Electrical Engineering Department, Technion. His research interests are statistical signal

processing, adaptive filtering, digital communications, and wideband array processing.



Israel Cohen (M'01–SM'03) received the B.Sc. (*summa cum laude*), M.Sc., and Ph.D. degrees in electrical engineering from the Technion—Israel Institute of Technology, Haifa, Israel, in 1990, 1993, and 1998, respectively.

From 1990 to 1998, he was a Research Scientist with RAFAEL Research Laboratories, Haifa, Israel Ministry of Defense. From 1998 to 2001, he was a Postdoctoral Research Associate with the Computer Science Department, Yale University, New Haven, CT. In 2001, he joined the Electrical Engineering

Department, Technion, where he is currently an Associate Professor. His research interests are statistical signal processing, analysis and modeling of acoustic signals, speech enhancement, noise estimation, microphone arrays, source localization, blind source separation, system identification, and adaptive filtering. He is a coeditor of the Multichannel Speech Processing section of the *Springer Handbook of Speech Processing* (Springer, 2008), a coauthor of *Noise Reduction in Speech Processing* (Springer, 2009), and a coeditor of *Speech Processing in Modern Communication: Challenges and Perspectives* (Springer, 2010).

Dr. Cohen is a recipient of the Alexander Goldberg Prize for Excellence in Research, and the Muriel and David Jacknow award for Excellence in Teaching. He served as an Associate Editor of the IEEE TRANSACTIONS ON AUDIO, SPEECH, AND LANGUAGE PROCESSING and the IEEE SIGNAL PROCESSING LETTERS, and as Guest Editor of a special issue of the *EURASIP Journal on Advances in Signal Processing* on Advances in Multimicrophone Speech Processing and a special issue of the *EURASIP Speech Communication Journal* on Speech Enhancement. He was general cochair of the 2010 International Workshop on Acoustic Echo and Noise Control (IWAENC).



Miriam A. Doron (S'90–M'93) received the B.Sc and M.Sc. degrees from the Technion—Israel Institute of Technology, Haifa, in electrical engineering in 1983 and 1986, respectively, and the Ph.D. degree in electrical engineering from the Tel-Aviv University, Tel-Aviv, Israel, in 1992.

In 1983, she joined RAFAEL, Haifa, as a Research Scientist and Section Head of the Signal Processing and Acoustics Department, and later on as a Research Fellow. She has been involved in R&D work on novel signal and array processing for atmospheric and under

water acoustic systems. Her areas of interest include statistical signal processing, adaptive array processing, spatial localization, classification of acoustic signatures, and acoustic communication.